ELSEVIER

Journal of Power Sources 110 (2002) 19–26

JOURNAL OF POWER SOURCES

www.elsevier.com/locate/jpowsour

Capacity fading mechanism for oxygen defect spinel as a 4 V cathode material in Li-ion batteries

Xiaoqing Wang, Hiroyoshi Nakamura, Masaki Yoshio*

Department of Applied Chemistry, Saga University, 1 Honjo, Saga 840-8502, Japan

Received 29 August 2001; received in revised form 12 December 2001; accepted 25 March 2002

Abstract

A series of cathode spinel materials with the nominal composites $Li_{1+x}Mn_{2-x}O_{4-z}$ have been studied with respect to capacity fading at room temperature upon cycling, both before and after elevated temperature storage. It was found that capacity fading is closely related to oxygen defect degree. The greater the oxygen deficiency, the poorer the cycling performance. Two major factors exist controlling the oxygen deficiency. One factor is oxygen loss at high synthesis temperature or upon cycling to high upper voltage, which increases the oxygen defect degree in samples. The other is Mn dissolution into the electrolytes accompanied by decrease in the oxygen deficiency. The latter one is supported by low temperature DSC and XRD data indicating that the temperature-dependent phase transition from cubic to lower symmetry becomes slight for oxygen defect samples after 60 °C storage.

Keywords: Li-ion battery; Spinel; Capacity fading; Oxygen deficiency; Phase transition

1. Introduction

As an alternative cathode material for $LiCoO_2$ and $LiNiO_2$, $LiMn_2O_4$ possesses several advantages, such as low cost due to its abundance in nature, no toxicity and a simple preparation process [1]. Nevertheless, its practical commercialization nowadays is still limited due to capacity fading upon cycling or at elevated operating temperature. Numerous works have been performed relevant to the capacity fading mechanism [2–6]. The common propositions are described as the following: (1) Mn slow dissolution into the slightly acidy electrolyte based on a disproportional reaction $2Mn^{3+} \rightarrow Mn^{4+} + Mn^{2+}$; (2) electrolyte oxidization on the surface of the charged electrode; (3) Jahn–Teller distortion at the deeply discharged state where the Mn average valence is lower than 3.5.

In our previous work [7], an additional discharge plateau at 3.2 V has been found for the oxygen defect samples. Importantly, the size of this plateau presents a strong dependence on the oxygen defect degree, represented by the z value in $Li_{1+x}Mn_{2-x}O_{4-z}$. The plateau increases with a rise in the z value, namely, a decrease of oxygen content. Based on this point, we have reported here the extensive investigation of capacity fading mechanism in terms of oxygen stoichiometry $(4-z)$. The results indicate that the oxygen defect degree in initial samples has a close relation with capacity fading, both before and after storage. It can also be found that oxygen defect degree is reduced as a result of Mn dissolution during elevated temperature storage. However, as reported by Gao and Dahn [8,9], oxygen loss due to strong oxidizing delithiated cathode during the high voltage region caused capacity fading at room temperature. A correlation likely exists between oxygen loss and Mn dissolution, since they have an opposite effect on oxygen content which considerably influences cycling performance. To solve this problem, we did some cycling tests under different temperatures in various voltage regions.

It has been reported recently that oxygen defect spinel cathode materials suffer from temperature-dependent phase transition from cubic to orthorhombic [10–12] or tetragonal [13–15]. In this work, to further ascertain the relation between the phase transition and oxygen deficiency, we studied the low temperature phase transition based on our samples, both before and after 1 week 60 °C storage.

2. Experimental

Mn_3O_4 and LiOH have been used as manganese and lithium sources, respectively to synthesize the samples by our melt-impregnation method [16]. The starting mixture

* Corresponding author. Fax: +81-952-28-8591.
E-mail address: yoshio@ccs.ce.saga-u.ac.jp (M. Yoshio).

0378-7753/02/$ – see front matter
PII: S0378-7753(02)00213-6

with a ratio of Li to Mn (1:2) is thoroughly ground and then heated at 450 and 530 °C, both for 5 h in air to obtain the disordered spinel structure. Such an intermediate was annealed over the temperature range of 700–850 °C in steps of 50 °C after a further grinding. Powder X-ray diffraction (XRD) was applied to characterize the crystal structure of final products and low temperature phase transition. XRD was carried out on a Rigaku RINT1000 X-ray diffractometer (Rigaku, Ltd., Japan) with Cu Kα radiation.

The chemical composition of each sample was precisely determined by using inductively coupled plasma (ICP) and automatic potentiometer titrator (Kyoto Electronics Manufacturing Co. Ltd., Japan). HCl and H_2O_2 were used to dissolve samples for detecting Li content by ICP. Total Mn and oxidation power of Mn were obtained by potential titration. In the case of oxidation power, the spinel samples were firstly dissolved in excess of $FeSO_4$ and once the Mn dissolved completely then the excess $FeSO_4$ was back-titrated with 1N $KMnO_4$ solution. For the total Mn, both Mn^{3+} and Mn^{4+} in the samples were reduced to Mn^{2+} in a mixture solution of HCl and H_2SO_4 under heating. This solution was titrated with 1N $KMnO_4$ around pH = 7. $Na_4P_2O_7$ was added to complex the oxidation product Mn^{3+}. The average oxidation state of Mn thus, was calculated from total Mn and oxidation power of Mn. The oxygen content $(4-z)$ was calculated based on the samples charge neutrality.

For the storage test, 3 g samples with 30 ml electrolyte solution were put into a Teflon bottle in dry room and stored in a 60 °C thermostat after being shaken thoroughly. After 1 week storage, this mixture was filtered to obtain the solid samples for chemical analysis.

The electrochemical characterization was operated on CR2032 coin cell. Cell assembly was carried out in an argon-filled dry box. The cell was comprised of a cathode and a lithium metal anode separated by a porous polypropylene film and glass fiber. The cathode consists of 20 mg active material and 10 mg Teflonized acetylene black (TAB) as a binding conductor. The mixture was pressed onto a stainless screen mesh at 400 kg/cm^2 and dried at 150 °C for 5 h in a vacuum glass tube. The electrolyte solution used is 1 M $LiPF_6$-ethylene carbonate (EC)/dimethyl carbonate (DMC) (1:2, v/v) with the water content less than 20 ppm. The cell was cycled in the voltage range of 4.7–3.0 and 4.3–3.5 V with typical current density 0.1 and 0.4 mA/cm^2, respectively.

DSC measurements were carried out on a computerized Perkin-Elmer DSC 7 calorimeter at a rate of 10 °C between the temperature −20 and 50 °C.

3. Results and discussion

Samples used here were identified by XRD patterns to be of pure cubic spinel structure. The composition analysis results are presented in Table 1. It can be clearly seen that the oxygen content $(4-z)$ gradually decreased from 3.995 to 3.981 as the heating temperature increased from 700 to 850 °C, corresponding to oxygen defect degree represented by z values from 0.005 to 0.019. This was due to the oxygen loss at higher temperature accompanied by the side reaction $Mn^{4+} \rightarrow Mn^{3+}$ [17]. Therefore, a slightly higher Mn^{3+} content and lower Mn^{4+} appeared at higher preparation temperatures, which agrees well with our analysis results as observed in Table 1. Sample D shows the largest amount of Mn^{3+} and thus, the strongest oxygen deficiency with a high z value of 0.019. This value is consistent with Sugiyama's results [18]. They reported the spinel samples with $\delta < 0.07$ in $LiMn_2O_{4-\delta}$ can keep pure cubic symmetry. Table 1 indicated that lower heating temperature contributes to optimizing oxygen stoichiometry of spinel material.

Since the oxygen deficiency was promoted by the higher heating temperature and led to an extra plateau at 3.2 V at the expense of capacity contained in the 4 V region as previously reported [7], then it is of much interest to study how the oxygen deficiency affects cycling behavior in the 4 V region.

The discharge capacities were plotted versus the cycle number in Fig. 1. The capacity can be easily observed to fade rapidly with the increasing oxygen deficiency. The relation between cycling performance and oxygen defect degree can be more clearly seen in Fig. 2, where the capacity retention after the first 50 cycles along with the oxygen defect degree z were described as a function of heating temperature. Sample A with the smallest oxygen deficiency $(z = 0.005)$ exhibits excellent cycleability with a low capacity loss 7.17% after the first 50 cycles whereas the poorest cycling performance for sample D losing 30.19% of initial capacity. This remarkable variation can be attributed to the structure instability of defect spinel structure during repeated Li-ion intercalation/deintercalation processing. Three-dimensional tunnel (comprised of 8a and 16c sites) for Li-ion diffusion thus, could be

Table 1
Chemical composition of samples before storage

Sample number	Heating temperature (°C)	Composition	Z in $(LiMn)_3O_{4-z}$	Li/Mn	Mn average valence
A	700	$Li_{1.010}Mn_{1.990}O_{3.995}$	0.005	0.507	3.507
B	750	$Li_{1.005}Mn_{1.994}O_{3.994}$	0.006	0.504	3.502
C	800	$Li_{1.010}Mn_{1.990}O_{3.988}$	0.012	0.507	3.500
D	850	$Li_{1.002}Mn_{1.998}O_{3.981}$	0.019	0.501	3.483

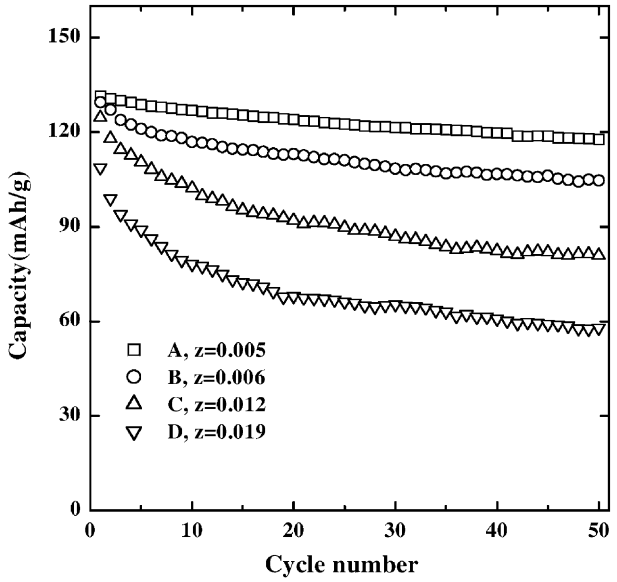

Fig. 1. Cycling behaviors for samples A, B, C and D, which were synthesized at different heating temperatures. Current density: 0.4 mA/cm^2; voltage region: 3.5–4.3 V; RT.

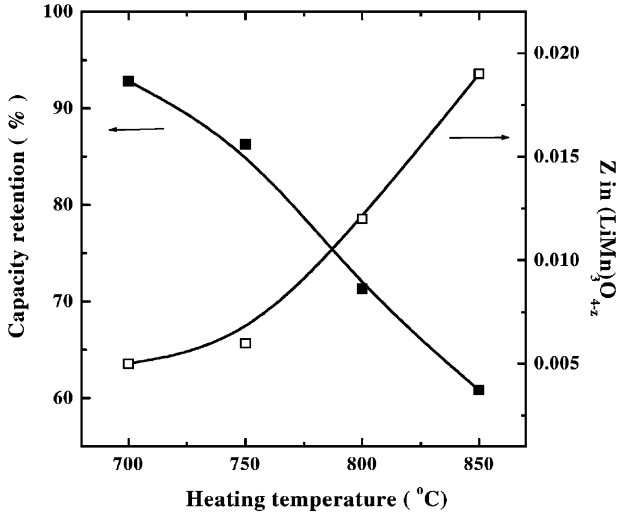

Fig. 2. Dependence of capacity retention after first 50 cycles and oxygen deficiency on the heating temperature for samples before storage. Current density: 0.4 mA/cm^2; voltage region: 3.5–4.3 V; RT.

somewhat damaged due to the oxygen deficiency. As determined by Kanno et al. [19], a small amount of interstitial oxygen was found to occupy 8b sites for the samples with oxygen vacancy at 32e. It is well known that 8b sites are vacant for stoichiometric cubic spinel. Therefore, it is very likely that the interstitial oxygen at 8b sites can impede Li-ion diffusion in the spinel cathode to a certain extent. High oxygen deficiency can cause a severe effect on Li-ion diffusion. The above results were obtained at room temperature. Thus, it can be speculated that the oxygen deficiency could be partly responsible for the capacity fading upon cycling at room temperature, which is proved by the following storage test.

To investigate the mechanism of capacity fading in samples with different oxygen deficiency at high temperature, we stored these samples in electrolyte with the ratio of 3 g/30 ml at 60 °C for 1 week. The stored samples named A1, B1, C1 and D1, respectively, were chemically analyzed. From the analysis results (Table 2), it can be observed that Mn content considerably decreased compared to that prior to storage whereas Li content increased as indicated by Li/Mn change and thus, the $Li_{1+x}Mn_{1-x}O_4$ formed. Mn average valance rose from about 3.5 to over than that. All of these changes origin from Mn^{3+} dissolution. As reported previously [20,21], Mn^{3+} dissolution is induced by HF generated from $LiPF_6$ electrolyte, which is sensitive to moisture. Mn^{3+} losses were determined to be 10.1, 8.32, 6.85 and 7.20% for samples A, B, C and D, respectively. This reduction trend is closely associated with the surface area and oxygen deficiency. It is well known that lower heating temperatures enhance the surface area of samples and subsequently induce Mn dissolution by enlarging the interface between the samples and the electrolyte. The Mn loss becomes severe for sample A and B, which were prepared at temperatures lower than 800 °C, due to the relatively high surface area 3.8144 and 1.8506 m^2/g, respectively, as shown in Fig. 3. Their specific capacities thus, significantly faded correspondingly as described later (Fig. 5). More interestingly, we found that with the Mn dissolution, the oxygen content $(4-z)$ in four samples increased to be close to stoichiometry, namely, the oxygen deficiency declined with z value of 0.002, 0.003, 0.005 and 0.008 for sample A1, B1, C1 and D1, respectively, compared to the original value of 0.005, 0.006, 0.012 and 0.019 before storage. Fig. 4 shows the effect of Mn dissolution on the XRD patterns. It can be observed that all the samples maintain cubic symmetry after storage whereas the peak intensity becomes weak and peaks are broadened compared to that before storage. It is evident that the variation amplitude shows close relation with Mn dissolution. As a result of $Li_{1+x}Mn_2O_4$ formation after

Table 2
Chemical composition of samples after 1 week 60 °C storage in 1 M $LiPF_6$-EC/DMC (1:2, v/v)

Sample number	Heating temperature (°C)	Composition	Z in $(LiMn)_3O_{4-z}$	Li/Mn	Mn average valence
A1	700	$Li_{1.041}Mn_{1.959}O_{3.998}$	0.002	0.531	3.551
B1	750	$Li_{1.024}Mn_{1.976}O_{3.997}$	0.003	0.518	3.526
C1	800	$Li_{1.018}Mn_{1.982}O_{3.995}$	0.005	0.513	3.518
D1	850	$Li_{1.011}Mn_{1.988}O_{3.992}$	0.008	0.508	3.508

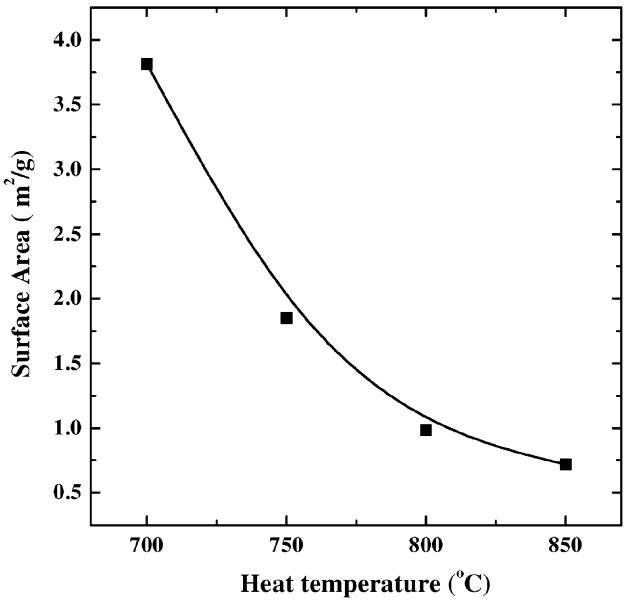

Fig. 3. Relation between surface area and preparation temperature for spinel samples.

storage, the cubic lattice constant a_0 shows decrease tendency for all samples as presented in the figure. This is caused by the larger radius for Mn^{3+} ions than Mn^{4+} ions.

The electrochemical performance must be affected due to the composition difference between before and after storage. The first cycle charge/discharge curves for all the samples before and after storage are shown in Fig. 5. Before storage,

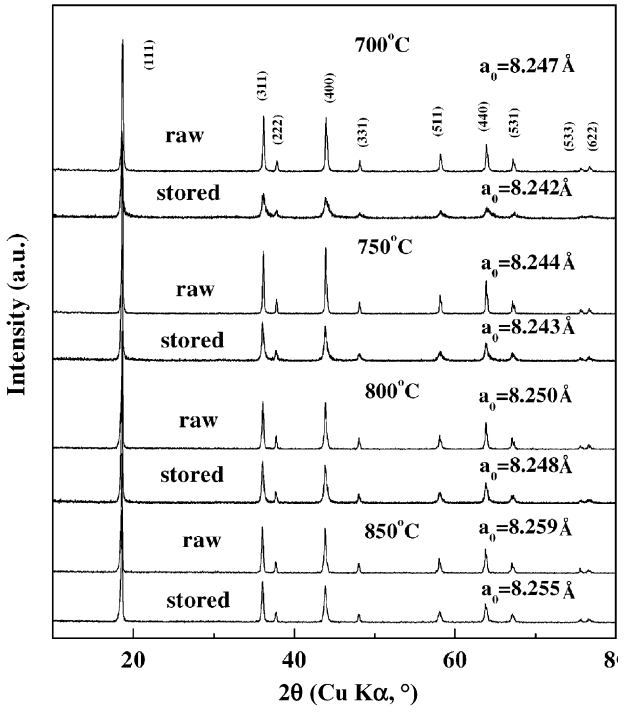

Fig. 4. XRD patterns for spinel samples prepared at different temperature before and after storage.

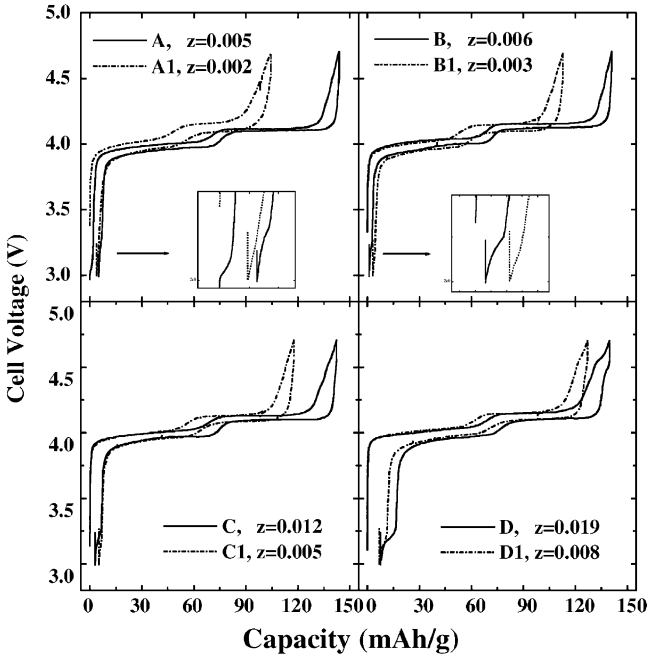

Fig. 5. First charge/discharge curves for samples before and after 1 week 60 °C storage. Current density: 0.1 mA/cm^2; voltage region: 3.0–4.7 V; RT.

the specific capacities of samples were degraded from nearly theoretical value of 143–139 mAh/g for sample A–D, respectively. In the discharge curves, an additional plateau appeared at 3.2 V and its amplitude increased with oxygen defect degree represented by z in $Li_{1+x}Mn_{2-x}O_{4-z}$ showing the same trends as that in our previous work [7]. In that work, capacity due to 3.2 V plateau is proportional to oxygen deficiency as $Cap_{3.2\,V} = 444z$ mAh/g. Consequently, this

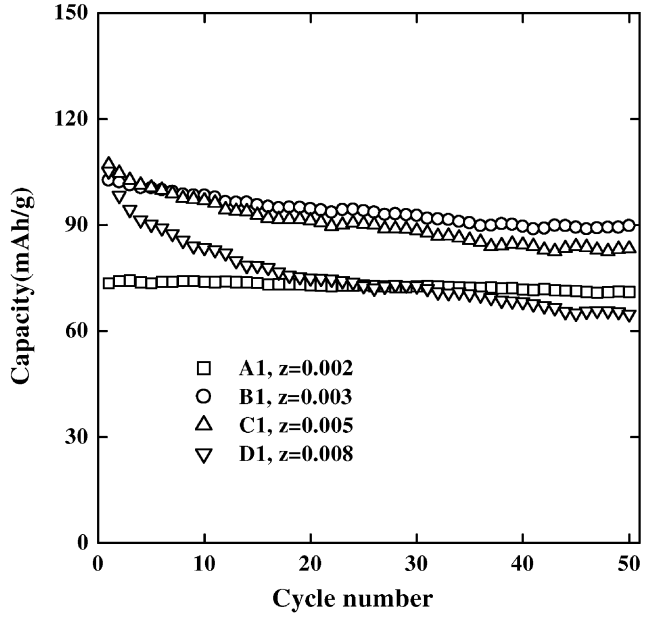

Fig. 6. Cycling behaviors for samples after 1 week 60 °C storage. Current density: 0.4 mA/cm^2; voltage region: 3.5–4.3 V; RT.

plateau becomes large gradually from sample A to sample D. The specific capacity loss during storage becomes small from sample A to D, corresponding to their Mn losses as the above mentioned. After storage, the 3.2 V plateau shrunk evidently compared to that before storage as shown in Fig. 5. Especially for sample A1 and B1, this plateau almost vanished. This tendency is in good agreement with oxygen deficiency decrease after storage. Such results can be a further evidence for our initial proposition that the 3.2 V plateau can serve as a useful index of oxygen defect degree. Thus, the cycling behavior at RT also changed into a better one than before 60 °C storage though having relatively low capacity (Fig. 6). Sample A1 retains almost 100% capacity after 50 cycles as opposed to sample A without storage, though suffering from rapid capacity fading from 143 to 127 mAh/g. Similarly, other sample B1, C1 and D1 also showed better cycling performance than sample B, C and D, respectively. The same relation exists between the oxygen deficiency and cycling properties as that before storage. Namely, samples with lower oxygen deficiency possess superior cycling properties to that with higher ones. This, therefore, suggests that minimizing the oxygen deficiency in samples can improve their cycling performance at room temperature. On the other side, superior cycling properties is also consistent with the fact that Li-ion content increased after storage. The excess Li in $Li_{1+x}Mn_{2-x}O_{4-z}$ $(0 < x < 1)$ can usually improve the rechargeability by stabilizing the spinel structure according to our previous results [22], in which we found that for Li-rich materials $Li_{1+x}Mn_{2-x}O_{4-z}$ $(0 < x < 1)$ and its charge and discharge process proceeds in the homogeneous phase reaction. Thus, the spinel structure can retain perfect integrity during repeated Li-ion intercalation/deintercalation. This point has been further proved by Xia et al. [23]. In present case, the excess Li occupied 16d sites arising from Mn^{3+} dissolution. As described in the disproportional reaction $2Mn^{3+} \rightarrow Mn^{4+} + Mn^{2+}$ [24], the soluble Mn^{2+} would go into electrolyte thus providing some vacant 16d sites for excess Li. Therefore, the integrity of spinel structure can be retained by excess Li. It should be noted that the extra plateau around 4.5 V during charge/discharge also shows close relation with oxygen deficiency (z value). Moreover, it shrunk after storage as 3.2 V plateau. Thus, we infer that occurrence of 4.5 V plateau origins from oxygen deficiency (z value).

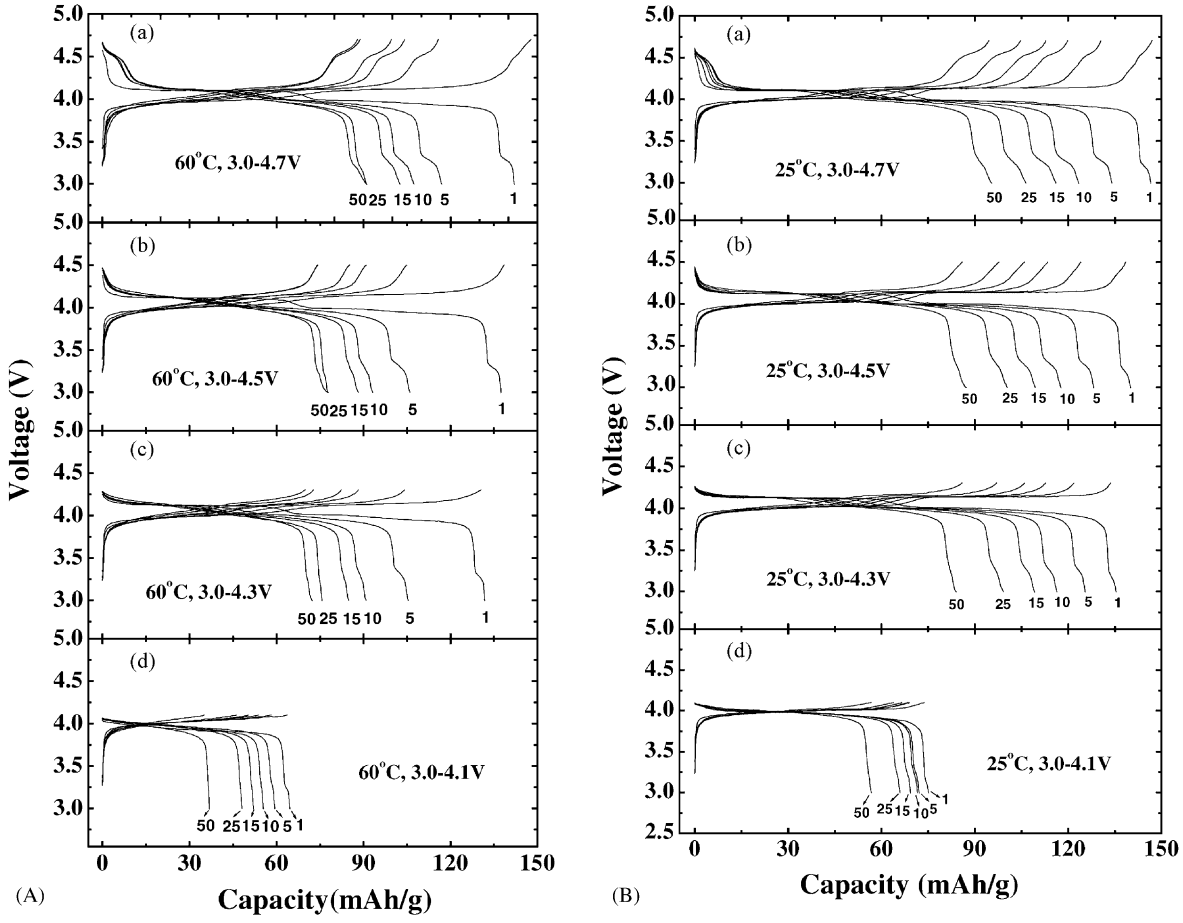

Fig. 7. (A) 3.2 V pleteau variation upon cycling with the different upper voltage for sample C (a) 3.0–4.1 V; (b) 3.0–4.3 V; (c) 3.0–4.5 V; (d) 3.0–4.7 V. The cycle numbers are shown in the figure. Current density: 0.1 mA/cm^2; RT. (B) 3.2 V pleteau variation upon cycling with the different upper voltage for sample C (a) 3.0–4.1 V; (b) 3.0–4.3 V; (c) 3.0–4.5 V; (d) 3.0–4.7 V. The cycle numbers are shown in the figure. Current density: 0.1 mA/cm^2; 60 °C.

The above results indicated that high temperature storage caused serious Mn loss leading to capacity fading. Meanwhile the oxygen defect degree was reduced due to the Mn dissolution. Therefore, it also implies that if the Mn dissolution dominates the capacity fading upon cycling at high temperature, with Mn slow dissolution into the electrolytes, the 3.2 V plateau size should become smaller and smaller during cycling. To verify this suggestion, sample C with much deficiency was utilized to carry out a series of cycling tests to various upper voltage at 60 °C and RT as shown in Fig. 7A and B, respectively. The results were discussed in several respects as follows. 3.2 V plateau in the first cycle decreased gradually with the decrease of upper voltage from 4.7 to 4.1 V at both 60 °C and RT. The 3.2 V plateau size when cycling between 3.0 and 4.7 V at 60 °C showed no reduction within the initial cycles (Fig. 7A). Contrary to our expectation, it increased slightly with cycle number when the upper voltage is higher than 4.3 V. Correspondingly, 4 V plateaus become smaller. This indicated that oxygen deficiency degree becomes high most likely due to oxygen loss occurring at the high voltage as investigated by Gao and Dahn [9]. They suggested that the electrolyte molecule provides the electron to the partially delithiated spinel cathode, thus, inducing the oxygen loss from the spinel. The higher upper voltage promoted this process. It can be clearly seen that the 3.2 V plateau in the first cycle gradually increased with rise of the upper voltage from 4.1 to 4.7 V with a further enhancement at 60 °C (Fig. 7A) with comparison to that at RT (Fig. 7B). These results agree well with those reported by Dahn. Controlled by two conflicting factors in terms of opposite influence on oxygen content, the oxygen deficiency obtained was still larger in the initial cycles as shown in Fig. 7A. Therefore, oxygen loss in the high voltage region can be another critical factor responsible for capacity fading besides Mn dissolution. On further cycling, the 3.2 V plateau ceases to increase but becomes smaller and smaller. Especially, this extra plateau vanishes eventually when the upper voltage is equal to 4.3 V and almost vanished from the 5th cycle for 4.1 V. This result is in good accordance with the above suggestions. However, not only simple Mn dissolution, but also oxygen loss affected the 3.2 V plateau. Thus, the shrinkage of this plateau upon further cycling can be interpreted by that the former factor prevails the latter one or some factors else cooperate during deeply cycling. At this stage, this phenomenon cannot be explained much clearly yet. It can also be found that high temperature can accelerate this variation by promoting Mn dissolution, which results in decrease of oxygen deficiency. It also can be concluded that Mn dissolution mainly takes place at high temperature and in the lower voltage region where the Mn^{3+} concentration is relatively higher than higher voltage region. However, oxygen loss mainly occurs in the high voltage region either at RT or HT. From these results, it can be concluded that the 3.2 V plateau size is associated not only with the oxygen defect degree in the initial spinel samples but also with the voltage range (mainly the upper voltage) and operating temperature.

Experimental results indicated that oxygen loss and Mn dissolution, both enhanced by elevated temperatures are different factors leading to poor cycling performance. Oxygen loss over the high voltage regions plays a major role contributing to capacity fading at room temperature whereas Mn dissolution mainly occurs in the low voltage range at elevated temperature.

As recently reported, oxygen defect spinels suffer from temperature-dependent phase transition from cubic to lower symmetry orthorhombic [10–12] or tetragonal structure [13–15]. In [13–15], the oxygen deficiency was adjusted by additional heat treatment of the spinel samples in air or N_2 and varying Li/Mn ratio in starting material. In our samples, oxygen deficiency was available by gradual increase of synthesis temperature and reduced by lowering final annealing temperature or by 1 week 60 °C storage. In view of the different way to get oxygen deficiency, we studied the low temperature DSC on our samples before and after storage to check the above-mentioned suggestion. Fig. 8 described the DSC results. It can be clearly observed that one exothermic peak appears between 10 and 15 °C on cooling and one endothermic peak on heating for oxygen defect sample D ($z = 0.019$), which indicate phase transition taking place in sample D close to room temperature. The former peak is much higher and sharper than the latter one.

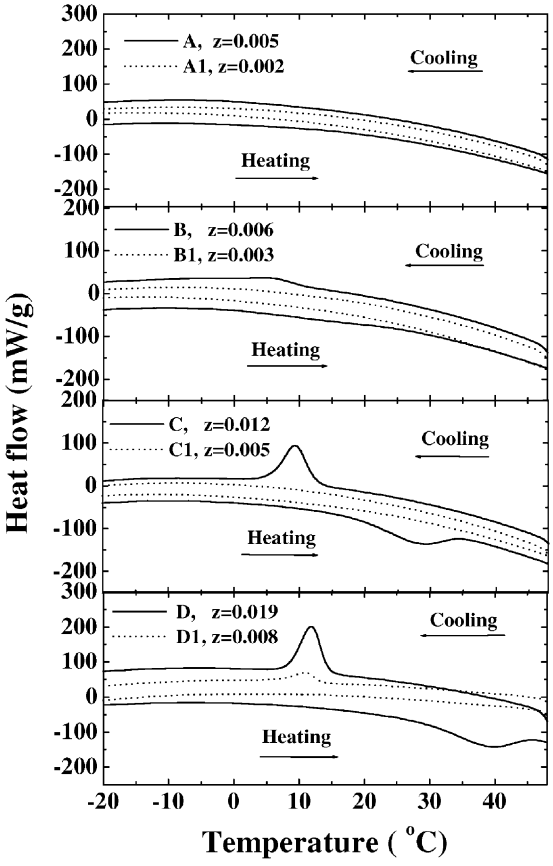

Fig. 8. Low temperature DSC for spinel samples A, B, C, D, A1, B1, C1, and D1.

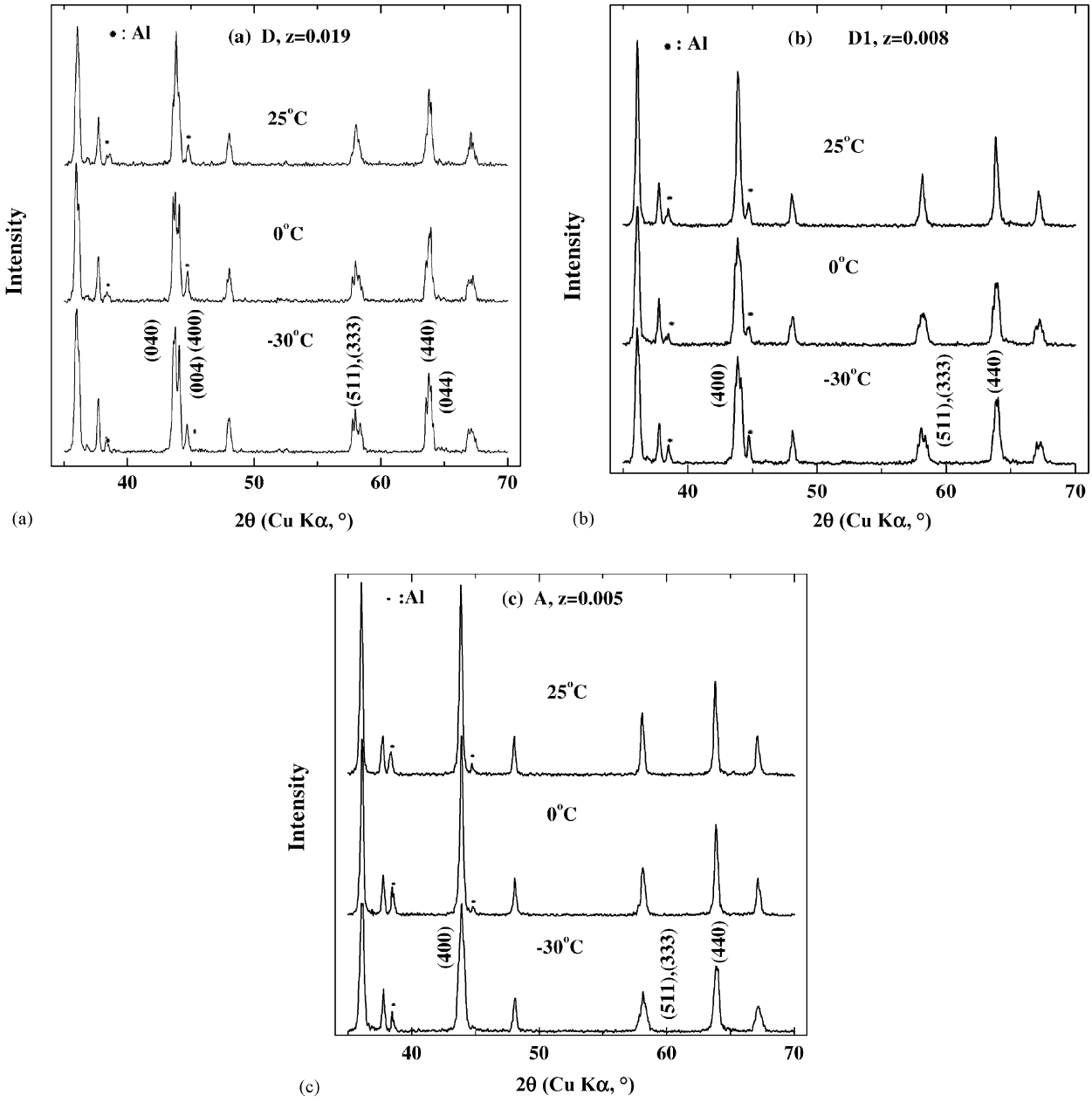

Fig. 9. XRD patterns at 25, 0 and −30 °C for 850 °C sample before storage (a), after storage (b) and 700 °C sample before storage (c).

This difference could be associated with the low reversibility degree for phase transition. After storage, both of the two peaks became smaller for sample D1 ($z = 0.008$). Interestingly, the amplitude of these peaks gradually reduced with increase of oxygen defect degree (z-value) and the phase transition temperature shifts to a higher one in the case of samples with more oxygen deficiency. Sample D has stronger peaks, both on cooling and on heating while the peaks disappear completely for samples with $z < 0.006$. The dependence of low temperature phase transition on oxygen defect degree is in good agreement with previous reports [11,13–15]. Thus, we suggest that phase transition occurs in samples with oxygen deficiency despite before or after storage and elevated temperature storage can minimize degree of phase transition by reducing the oxygen deficiency. The main factor contributing to phase transition is oxygen deficiency. This point is not conflicting with results of Yamada [25,26]. They suggested that the phase transition takes place in spinels with Mn valence <3.6 due to Jahn–Teller distortion. In the case of their samples, oxygen content will decrease due to Mn valence reduction and thus, becomes deficient, which consequently causes phase transition. Furthermore, their sample $LiMn_2O_4$ shows cubic symmetry while another sample $LiMn_2O_{3.86}$ adopts tetragonal one at room temperature. This result is in good agreement with our data that the more oxygen deficiency, the higher the phase transition temperature.

To further investigate the low temperature-dependent phase transition, we have conducted XRD at various temperatures for samples D, D1 and A as plotted in Fig. 9. In the case of sample D with more oxygen deficiency, the peaks (400), (511)/(333) and (440) become triplets at 0 and −30 °C. The peaks split shows that phase transition occurs at low temperature. The new phase has been suggested to be two different types. One is a mixture of the new tetragonal phase and original cubic phase proved with synchrotron XRD by Yang et al. [15] and the other is orthorhombic phase confirmed with neutron powder diffraction [10–12]. In Fig. 9, the degree of peak split becomes more severe at −30 °C than at 0 °C. In other words, phase transition depends on temperature and this, meanwhile implies that low-temperature phase is not a single new one, but a mixture as reported by Yang et al. For the stored sample D1 ($z = 0.008$), only a slight peak split can be found at −30 °C and an even slighter one at 0 °C. For sample A ($z = 0.005$), although asymmetric broadening is observed for peaks (400), (511)/(333) and (440), no detectable peak split occurs at low temperature. This agrees well with the DSC results. Since the −30 °C phase is different from the usual cubic one at room temperature, which means the structural deterioration taking place between RT and −30 °C, then when subjected to cooling or heating during this temperature range the samples with oxygen defect inevitably suffer from phase transformation resulting in heat effect as depicted in low temperature DSC data. Therefore, we believe that the oxygen deficiency causes phase transition at lower temperature and the transition temperature depends strongly on the degree of oxygen deficiency. Namely, samples with much oxygen deficiency undergo phase transition at higher temperature than those with slight oxygen deficiency and no phase transition takes place in nearly oxygen stoichiometric samples. Phase transition close to room temperature for severely oxygen defective spinel samples could be a potential factor responsible for poor cycling performance at room temperature.

Therefore, it can be concluded that phase transition strongly depends on oxygen defect degree, despite how the oxygen deficiency is generated.

4. Conclusion

Oxygen defect spinel samples were used to investigate the capacity fading mechanism. It was found that the degree of oxygen deficiency shows a strong relationship with the cycling properties. Mn dissolution during 60 °C storage reduced the oxygen deficiency for samples either with high or low oxygen deficiency. Mn dissolution and oxygen loss arising from both cycling to high upper voltage and high preparation temperature would considerably contribute to the capacity fading during cycling at elevated temperature. Phase transition takes place in the oxygen defect spinel close to room temperature despite the oxygen deficiency producing way. No phase transition occurs in nearly stoichiometric oxygen spinel samples. The more the oxygen deficiency is, the higher temperature the peak position in DSC shifts to and the higher the peak is. All the results suggest some ways to improve cycling performance, both at RT or HT by lowering the preparation temperatures or minimizing the interface between the cathode and electrolyte in order to avoid oxygen deficiency or to minimize the Mn dissolution.

Acknowledgements

The authors would like to thank the grants in aid for Scientific Research from the Japanese Ministry of Education (No. 06555188) for partial support of this research work.

References

[1] J.M. Tarascon, D. Guyomard, J. Electrochem. Soc. 138 (1991) 2864.
[2] R.J. Gummow, A. de Kock, M.M. Thackery, Solid State Ionics 69 (1994) 59.
[3] Y. Xia, M. Yoshio, J. Power Sources 66 (1997) 129.
[4] Y. Xia, Y. Zhou, M. Yoshio, J. Electrochem. Soc. 144 (1997) 2593.
[5] G.G. Amtucci, A. Blyr, C. Schmutz, J.M. Tarascon, Progr. Batt. Mater. 16 (1997) 1.
[6] H. Huang, C.A. Vincent, P.G. Bruce, J. Electrochem. Soc. 146 (1999) 481.
[7] X. Wang, Y. Yagi, Y.-S. Lee, M. Yoshio, Y. Xia, T. Sakai, J. Power Sources 4325 (2001) 1.
[8] Y. Gao, J.R. Dahn, J. Electrochem. Soc. 143 (1996) 100.
[9] Y. Gao, J.R. Dahn, Solid State Ionics 84 (1996) 33.
[10] K. Oikawa, T. Kamiyama, F. Izumi, B.C. Chakoumakos, H. Ikuta, M. Wakihara, J. Li, Y. Matsui, Solid State Ionics 109 (1998) 35–41.
[11] R. Kanno, M. Yonemura, T. Kohigashi, Y. Kawamoto, M. Tabuchi, T. Kamiyama, J. Power Sources 97/98 (2001) 423–426.
[12] G. Rousse, C. Masquelier, J. Rodríguez-Carvajal, M. Hervieu, Electrochem. Solid State Lett. 2 (1) (1999) 6–8.
[13] Y. Xia, T. Sakai, T. Fujieda, X. Yang, X. Sun, Z.F. Ma, J. McBreen, M. Yoshio, J. Electrochem. Soc. 148 (2001) A723.
[14] M. Yoshio, Y. Xia, T. Sakai, Jpn. Electrochem. 69 (2001) 516.
[15] X. Yang, X. Sun, M. Balasubramanian, J. McBreen, Y. Xia, T. Sakai, M. Yoshio, Electrochem. Solid State Lett. 4 (2001) A117.
[16] M. Yoshio, S. Inoue, M. Hyakutake, G. Piao, H. Nakamura, J. Power Sources 34 (1991) 147.
[17] V. Manev, A. Momchilov, A. Nassalevska, A. Kozawa, J. Power Sources 43/44 (1993) 551.
[18] J. Sugiyama, T. Atsumi, T. Hioki, S. Noda, N. Kamegashira, J. Power Sources 68 (1997) 641–645.
[19] R. Kanno, A. Kondo, M. Yonemura, R. Gover, Y. Kawamoto, M. Tabuchi, T. Kamiyama, F. Izumi, C. Masquelier, G. Rousse, J. Power Sources 81/82 (1999) 542–546.
[20] D.H. Jang, Y.J. Shin, S.M. Oh, J. Electrochem. Soc. 143 (1996) 2204.
[21] D.H. Jang, S.M. Oh, J. Electrochem. Soc. 144 (1997) 3342.
[22] M. Yoshio, H. Noguchi, T. Miyashita, H. Nakamura, A. Kozawa, J. Power Sources 54 (1995) 483–486.
[23] Y. Xia, M. Yoshio, J. Electrochem. Soc. 143 (1996) 825.
[24] R.J. Gummow, A. De Kock, M.M. Thackery, Solid State Ionics 69 (1994) 59.
[25] A. Yamada, M. Tanaka, Mater. Res. Bull. 30 (1995) 715.
[26] A. Yamada, J. Solid State Chem. 122 (1996) 160.